DOI: 10.13009/EUCASS2017-472

Accurate positioning of multirotor UAVs for civil infrastructure monitoring

D. Di Bacco[⋆]*, M. Giurato*[⋆] *and M. Lovera*[⋆†]
[⋆]*Dipartimento di Scienze e Tecnologie Aerospaziali, Politecnico di Milano*
Via La Masa 34, 26900 Milano, Italy

[†]Corresponding author

Abstract

in this paper a comparison of fixed-point position control performance for a quadrotor and a quad-tilt-arm is presented and discussed, in terms of the problem of accurate distance holding of the UAV from a vertical surface in the presence of wind, which is a critical task for automatic monitoring of large civil infrastructures.

1. Introduction

Nowadays, the use of multirotor platforms as Unmanned Aerial Vehicles (UAVs) is rapidly increasing,[6,11] as multirotors can provide simple and reliable solutions for short-range missions in a number of civil applications, such as, *e.g.*, aerial photography, security, agriculture, structural health monitoring (SHM) of large infrastructures and so on. Regarding this latter application area, to carry out SHM missions for buildings and industrial plants to gather reliable data, the ability of accurate fixed-point position control in the presence of disturbances (such as, *e.g.*, wind gusts in the proximity of large civil structures) is a significant requirement. In this respect, the main drawback of conventional multirotors is that they are intrinsically under-actuated, *i.e.*, no matter how many rotors they carry (*e.g.*, quadcopters, hexacopters, octocopters), they cannot achieve full decoupled control on the 6 degrees of freedom (DoFs) of the vehicle, so that to respond to, say, longitudinal disturbances, the pitch attitude of the platform must be also perturbed, thus causing a needlessly complex and slow response. It is thus clear that aerial platforms overcoming the flying limits of classical multirotors could increase the exploitation of UAVs in various fields. In view of this, many alternative configurations have been studied in recent years, including tilting rotors.[1,10] Such solution can produce lateral forces by rotating the thrust vectors around fixed axes in order to obtain the possibility to achieve forward flight with level attitude, or to change the attitude of the quadrotor while hovering at a fixed point. Therefore, in the case of a quad-tilt-arm, the flight control system can rely on 4 + 4 control variables (rotor rpms and rotor tilt angles) which can be used to achieve more accurate fixed-point position control exploiting the faster disturbance attenuation capability provided by the tilting rotors.

In view of the above discussion, in this paper a comparison of fixed-point position control performance for a quadrotor and a tilt-arm platform is presented and discussed, in terms of the problem of distance holding of the UAV from a vertical surface. For both platforms, a Kalman filter is used for state estimation, which realizes a fusion between data coming from the on-board sensors, *i.e.*, the accelerometer and the ultrasonic proximity sensor. On the other hand, robust control laws, optimally tuned with structured H_∞ synthesis, are used to handle the attitude and position dynamics of the UAVs in both configurations: for the quadrotor, a conventional backstepping architecture is used, while for the quad-tilt-arm rotor rpms are used to control attitude while rotor tilting angles are used for position control. The performance of the two platforms is evaluated and verified in simulation, in response to aerodynamic disturbances that can occur during the flight, such as wind gusts and/or turbulence.

The paper is organised as follows: the dynamic model for the formulation of the position control problem is first derived; then the statement of the position control problem is given, both for a quadrotor and a tilt-arm platform and the control design approach for both platform is described. Finally, simulation results are presented and discussed.

2. Models for position dynamics

2.1 Quadrotor model

In the present work, the longitudinal dynamics of the quadrotor is studied, assuming for the sake of simplicity that the vertical surface to be inspected is in the North direction. Therefore the platforms are equipped with a proximity sensor aligned with the longitudinal body axis. For the quadrotor, a rigid body model for translational motion can be written as

$$\begin{bmatrix} \dot{u} \\ \dot{v} \\ \dot{w} \end{bmatrix} = \begin{bmatrix} vr - qw \\ wp - ur \\ uq - vp \end{bmatrix} + g \begin{bmatrix} -\sin(\Theta) \\ \sin(\Phi)\cos(\Theta) \\ \cos(\Phi)\cos(\Theta) \end{bmatrix} - \begin{bmatrix} 0 \\ 0 \\ \frac{T}{m} \end{bmatrix}, \tag{1}$$

where u, v, w and p, q, r are, respectively, the body components of the linear and angular velocity of the platform, Φ and Θ are the roll and pitch angles and T is the overall thrust (aligned with the z body axis). Selecting only the longitudinal dynamics one gets

$$\begin{aligned} \dot{x} &= u \\ \dot{u} &= vr - qw - g\sin\Theta. \end{aligned} \tag{2}$$

As only small deviations from the nominal position are of interest, equations (2) are linearised at $v = w = 0$, $p = q = r = 0$, $\Phi = \Theta = 0$, leading to

$$\begin{aligned} \dot{x} &= u \\ \dot{u} &= -g\Theta. \end{aligned} \tag{3}$$

The dynamic system with two states and a single input Θ can be therefore rewritten in a matrix form as follows:

$$\begin{bmatrix} \dot{x} \\ \dot{u} \end{bmatrix} = \begin{bmatrix} 0 & 1 \\ 0 & 0 \end{bmatrix} \begin{bmatrix} x \\ u \end{bmatrix} - g \begin{bmatrix} 0 \\ 1 \end{bmatrix} \Theta. \tag{4}$$

2.2 Tilt-arm model

The main difference between the tilt-arm platform and the quadrotor is that the translational dynamics is decoupled from the attitude of the UAV by actuating the tilting arms. Recalling the translational dynamics and rearranging it for a single axis, one gets

$$\begin{aligned} \dot{u} &= \frac{1}{m} F_x = \\ &= \frac{1}{m}(-K_T \sin(\alpha_2)\Omega_2^2 + K_T \sin(\alpha_4)\Omega_4^2), \end{aligned} \tag{5}$$

where F_x denotes the longitudinal component of thrust arising due to the tilting of the left and right rotors (respectively, number 2 and number 4, with tilt angles α_2, α_4 and rotor rpms Ω_2, Ω_4) and K_T is an aerodynamic parameter which can be either computed using, *e.g.*, blade element theory or estimated from data.

In the above equation, the gravitational term does not appear since we are assuming null attitude angles and thus no gravitational force component is acting on the specified axis. Linearizing around a near hovering condition ($v = w = 0$, $p = q = r = 0$, $\Phi = \Theta = 0$ and $\Omega_2 = \Omega_4 = \Omega_h$) and assuming that $\alpha_2 = \alpha_4 = \alpha$, *i.e.*, that actuation of the tilting arms is symmetric, the model can be written as

$$\dot{u} = \frac{2K_T\Omega_h^2}{m}\alpha. \tag{6}$$

2.3 Measurement noise and estimation errors

Among the possible uncertainties present in the model, the noise measurements of the sensors have been considered because they inevitably affect the system and likely play a major role in determining its performance. Similarly, for states that are not measured directly but are rather estimated by the on-board navigation system, steady-state estimation errors have to be taken into account. Both measurement noise and estimation errors are described by means of their standard deviations. For position, in the North direction, the uncertainty is related to the accuracy of the proximity

DOI: 10.13009/EUCASS2017-472

Table 1 – Measurement noise on state variables.

State	Standard deviation σ	Unit
N	0.01	m
E	1.00	m
D	0.10	m
u	0.01	m/s
v	0.01	m/s
w	0.10	m/s
Φ	1.00	deg
Θ	1.00	deg
Ψ	1.00	deg
p	1.00	deg/s
q	1.00	deg/s
r	1.00	deg/s

sensor and is therefore of centimetrical order; along the Down direction the uncertainty is linked to the performance of the barometer and is therefore of the order of decimeters; towards East, on the other hand, uncertainty is much larger since it is due to the low accuracy of the GPS measurements and is therefore of the order of a meter. The standard deviations of the considered noise processes are summarized in Table 1.

2.4 Disturbances

Additional uncertainties in the model can be considered as environmental conditions in which the UAV operates such as turbulence and wind gusts. These factors are inserted into the system as external disturbance forces and moments. Therefore, to describe the wind's impact on the quadrotor motion a wind model is applied to account for the forces and moments acting on the platform, as shown in Figure 1.

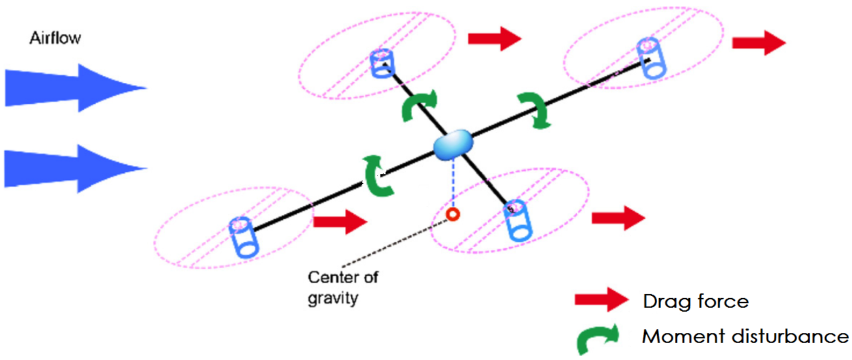

Figure 1 – Wind impact on quadrotor.

Aerodynamic drag acts mainly on the four rotors; since the platform is symmetric in the X-Y plane, the total drag can be modeled as a force[2] acting on the center of mass of the vehicle (thus no moments are created by drag) and given by

$$F_{dist} = -\frac{1}{2}\rho C_d A (V - V_w)^2 \cdot sgn(V - V_w) \tag{7}$$

where ρ is the air density, C_d is the drag coefficient, A is the platform's projected area in the corresponding plane, V is the speed and V_w is the wind speed. In particular, A depend on the axes with respect to which it is calculated:

$$A = \begin{bmatrix} A_x & 0 & 0 \\ 0 & A_y & 0 \\ 0 & 0 & A_z \end{bmatrix}. \tag{8}$$

It has been chosen to calculate the aerodynamic drag directly in the body frame since in this way the reference area is constant irrespectively of the orientation of the vehicle. As for the drag coefficient, it is reasonable to assume that quadrotors are symmetric about all three body axes, thus the drag constant is the same when flying in any direction along a body axis. The drag constant along each body axis can be unique and its main components are due to the rotors and to the body center, *i.e.*, around the center of mass of the UAV. More precisely, introducing some concepts of *Blade Element Theory* and *Moment Theory*,[5] a rotor drag coefficient can be defined with an empirical relation as

$$C_{d_{\text{rotor}}} = 0.0087 - 0.0216\bar{\alpha} + 0.4\bar{\alpha}^2, \tag{9}$$

where $\bar{\alpha}$ is the mean angle of attack of the blade, given by

$$\bar{\alpha} = \frac{6C_T}{C_{L_\alpha}}\frac{1}{\sigma} = \frac{6C_T}{2\pi}\frac{A_{disk}}{A_{blade}}, \tag{10}$$

where σ is the *solidity ratio*. The central body of the UAV can be treated as a sphere moving into the air; the aerodynamic drag coefficient can be obtained by a data correlation in fuction of Reynolds number as follows[8]:

$$C_{d_{\text{center}}} = \frac{24}{Re} + \frac{\frac{2.6Re}{5}}{1+(\frac{Re}{5})^{1.52}} + \frac{0.441(\frac{Re}{263000})^{-7.94}}{1+(\frac{Re}{263000})^{-8}} + \frac{Re^{0.8}}{461000}. \tag{11}$$

Moreover, considering a turbulent environment, the UAV is subject to angular rates caused by movement of the surrounding air mass and are thus considered as follows:

$$M_{dist} = -\begin{bmatrix} \frac{\partial L}{\partial p} & 0 & 0 \\ 0 & \frac{\partial M}{\partial q} & 0 \\ 0 & 0 & \frac{\partial N}{\partial r} \end{bmatrix} \begin{bmatrix} p_w \\ q_w \\ r_w \end{bmatrix}. \tag{12}$$

For an accurate description of external phenomena affecting multirotor flight, atmospheric conditions concerning wind speed were modeled as a stationary mean wind from a given direction to which gusts and turbulence are added according to

$$V_w = V_{w_{\text{mean}}} + V_{w_{\text{turb}}} + V_{w_{\text{gust}}}. \tag{13}$$

Transforming equation (13) to the body frame, the relative airspeed of the multirotor can be obtained and finally the aerodynamic forces and moments affecting the system can be computed. The wind modeling has largely been inspired by several works that deal with the same theme, mathematical representation in the Military Specification MIL-F-8785C[9] and Mathworks content on aerospace modeling[7]:

1. *Wind shear model:* a mean wind field is described by a magnitude W_{20} at 20 feet from the ground. As a result of wind shear, the resulting wind speed depends logarithmically on altitude. The mean wind speed is therefore calculated as

$$V_{w_{\text{mean}}} = W_{20}\frac{\ln\frac{h}{z_0}}{\ln\frac{20}{z_0}} \qquad 3\text{ ft} < h < 1000\text{ ft} \tag{14}$$

   where W_{20} is the wind speed at 20 ft altitude, h is the altitude and z_0 is a constant equal to 0.15 ft for Category C flight phases. A mean wind field of about 2 m/s in North direction has been simulated and included in the model.

2. *Dryden Wind Turbulence Model:* at altitudes lower than 1000 feet, which is well above the ceiling of a quadrotor, turbulence can be modelled as a stochastic process defined by its velocity spectra. The turbulence field is assumed to be frozen in time and space, with the implication that the response of the platform results from its motion relative to the turbulent field. Under this assumption, turbulence can be modelled as a one-dimensional field that involves just the three orthogonal velocity components taken at the platform's centre of gravity. The model takes white noise as an input and may be seen as a wide-sense stationary stochastic process, *i.e.*, it is time-invariant. The power spectral density (PSD) functions for the Dryden model define the contributions towards the turbulence across the frequency range; they describe the spectral density for a given height h, mean-wind relative airspeed V as well as a specific wind speed at 20 ft above the ground.

3. *Wind Gust Model:* a wind gust is a temporary increase in the mean wind speed. Its rate of increase is governed by the present wind speed, the vehicle airspeed and the increase length of the gust. A gust is commonly modeled to have a "1-cosine" shape according to the Military Specification MIL-F-8785C. The equation describing the gust is given by

$$V_{w_{\text{gust}}} = \begin{cases} 0 & x < 0 \\ \frac{V_m}{2}(1-\cos(\frac{\pi x}{d_m})) & 0 \le x \le d_m \\ V_m & x > d_m \end{cases} \tag{15}$$

DOI: 10.13009/EUCASS2017-472

where V_m is the gust amplitude, d_m is the gust length and x is the distance traveled. Note that the previous equation is not time-dependent and only describes the physical length of the gust. The duration for which an aircraft is exposed to the relative onset of a gust depends on the aircraft's current airspeed, where a faster airspeed will result in a quicker onset of the wind gust.

The total wind speed in the NED axes coming from equation (13) is shown in Figure 2 while the angular wind rates from the Dryden turbulence model are shown in Figure 3.

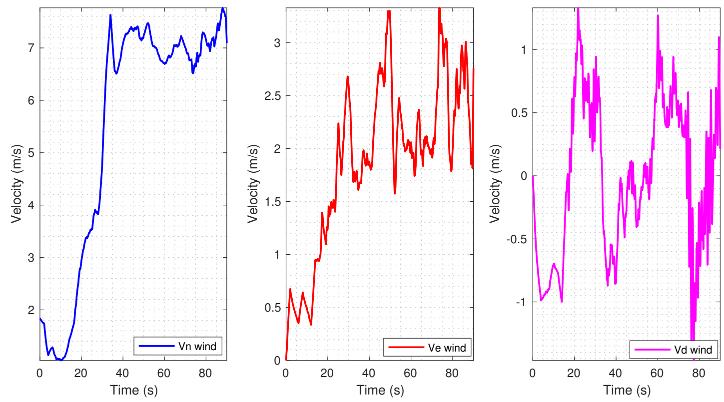

Figure 2 – Total wind speed.

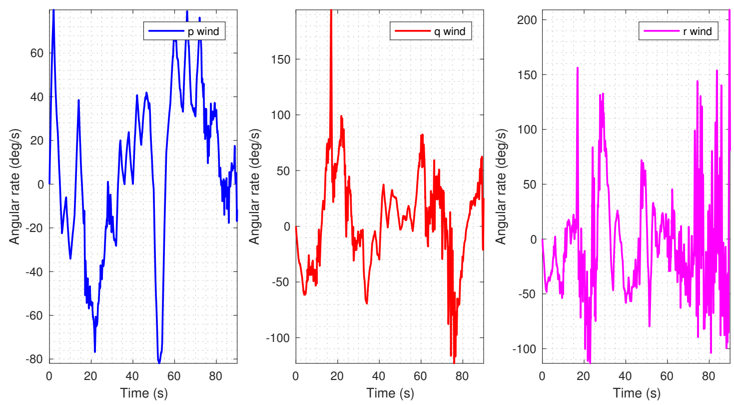

Figure 3 – Wind angular rates.

3. Position control architecture

The activation of the position hold control mode studied in this paper can be realised either by the pilot by means of a specific command when the platform has been positioned manually at the desired distance from the surface, or automatically when the position estimate provided by the navigation system falls below a certain threshold and is set as reference. Position control is carried out by the two platforms in different ways. For the quadrotor platform. the position control law modifies the attitude of the UAV, and is therefore affected by the limited bandwidth of the closed-loop attitude dynamics. For the tilt-arm platform, on the other hand, position control is obtained with level attitude, by varying the tilt angles of the arms. More precisely, in the case of the quadrotor the controller provides a correction pitch angle that eliminates the difference between real distance and desired distance of the UAV from the surface, while in the case of the tilt-arm the correction acts directly on the longitudinal force F_x by means of the tilt angle α.

Clearly, for such distance control to operate safely, the position control loop must be able to reach the setpoint in a slow and gradual way and, above all, without overshoot in order to maintain the UAV in a safe situation. In fact, an excessive overshoot, *e.g.*, due to disturbances, could cause a collision between the multirotor and the investigated surface.

DOI: 10.13009/EUCASS2017-472

3.1 Quadrotor position control

For the quadrotor, position control is realized by a cascade architecture, *i.e.*, with an inner loop on velocity and an outer loop on position, as shown in Figure 4.

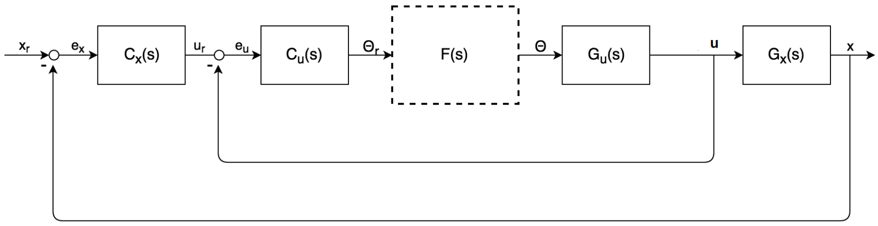

Figure 4 – Position control loops (quadrotor platform).

In the block diagram the position setpoint is denoted as x_r, u is the longitudinal speed of the quadrotor and x is its position. The pitch dynamics can be modeled by a transfer fuction $F(s)$ that receives as input the pitch reference angle and tracks it with an appropriate control law.[4] The regulator $C_u(s)$ is therefore designed for the subsystem $F(s)G_u(s)$ and it has to mitigate the effect of possible disturbances by ensuring that u tracks u_r with a faster dynamics than the desired closed-loop position dynamics. In other words, a high performance inner loop makes the effect of the disturbances negligible on the entire control system. Using equation (6) and transforming it into the Laplace domain, the following transfer functions are obtained:

$$\begin{aligned} G_u(s) &= \frac{U(s)}{\Theta(s)} = -\frac{g}{s} \\ G_x(s) &= \frac{X(s)}{U(s)} = \frac{1}{s}. \end{aligned} \tag{16}$$

Finally, blocks $C_x(s)$ and $C_u(s)$ are the PID controllers, with generic transfer functions given by

$$C(s) = K_p + \frac{K_i}{s} + \frac{K_d s}{sT_f + 1}. \tag{17}$$

3.2 Tilt-arm position control

The main difference between the tilt-arm platform and the quadrotor one is that the translational dynamics of the tilt-arm is decoupled from the attitude of the UAV by actuating the tilting arms; this translates, for the purposes of the model, in a different transfer function $G_u(s)$. Recalling the translational dynamics, the trnsfer function for the case of the tilt-arm is given by

$$G_u(s) = \frac{U(s)}{\alpha(s)} = \frac{2K_T\Omega_h^2}{m}\frac{1}{s}. \tag{18}$$

Moreover, the previously described $F(s)$ transfer function relative to the attitude dynamics does not play any role in this case and reduces to a gain introduced by the mixer matrix for the translational dynamics, given by

$$F(s) = \frac{1}{2K_T\Omega_h^2}. \tag{19}$$

The overall architecture of the traslational control for the tilt-arm configuration is shown in Figure 5.

4. H_∞ fixed-structure synthesis

In this study, the controller parameters have been tuned using structured H_∞ synthesis.[3] In general, as shown also in Figure 6, given a rational transfer function $P(s)$ and a structured controller $K(s,\theta)$ that depends on the tuning parameter vector θ, the structured H_∞ synthesis problem consists in looking for the parameters θ that minimize

$$\|T(s)_{w\to z}(P(s), K(s,\theta))\|_\infty, \tag{20}$$

DOI: 10.13009/EUCASS2017-472

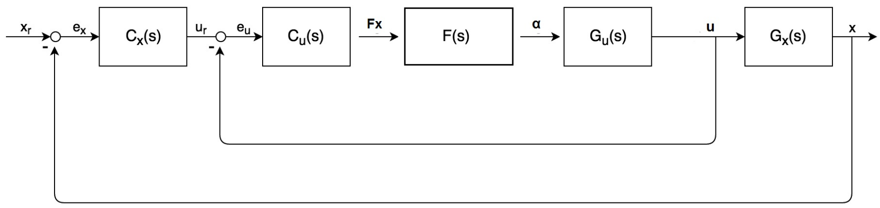

Figure 5 – Position control loops (tilt-arm platform).

where $T(s)_{w\rightarrow z}(P(s), K(s,\theta))$ is the closed-loop transfer function on the input-output channel $w \rightarrow z$, to be defined in the problem formulation to represent the relevant stability nd performance requirements. External inputs as references or disturbances are contained in w, while the outputs related to performance indices, for example the error signals, are stored in z.

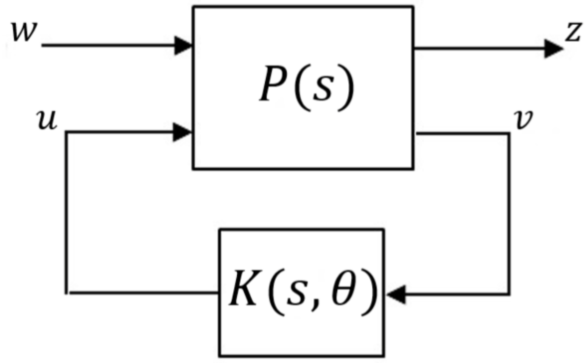

Figure 6 – H_∞ regulation scheme.

More precisely, tracking performance (in terms of error and settling time) and disturbance rejection requirements have been formulated as follows.

- Tracking requirements: the closed-loop system (from x_r to x) must have a maximum relative steady-state error equal to 0.0001%, a maximum relative peak error of 1% and be able to track reference signals within the 0.2 rad/s bandwidth. This last requirement defines the rise time of the system; indeed the two parameters are related by $T_s = \frac{2}{\omega_c}$. The criterion corresponding to this requirement is given by

$$J(\theta) = \left\| \frac{1}{\text{MaxError}} (F(s,\theta) - 1) \right\|_\infty \tag{21}$$

  where $F(s,\theta)$ is the closed-loop transfer function from x_r to x and the maximum error profile is defined as

$$\text{MaxError} = \frac{(\text{PeakError})s + \omega_c(\text{DCError})}{s + \omega_c}. \tag{22}$$

- Disturbance rejection requirements: it is imposed that the sensitivity function $S(s)$ satisfies the disturbances attenuation requirement with respect to a specific shaping function $W(j\omega)$ over the range of frequencies of interest (Ω):

$$J(\theta) = \max_{\omega\in\Omega} \|W(j\omega)S(j\omega,\theta)\|_\infty. \tag{23}$$

Figures 7-8 provide graphical representations of the requirement bounds listed above for the quadrotor and the tilt-arm platforms and present the achieved closed-loop performance. As can be seen from the figures, and as expected from the dynamic analysis in the previous section, the tilt-arm platform can provide closed-loop position control with a significantly better performance with respect to the quadrotor.

DOI: 10.13009/EUCASS2017-472

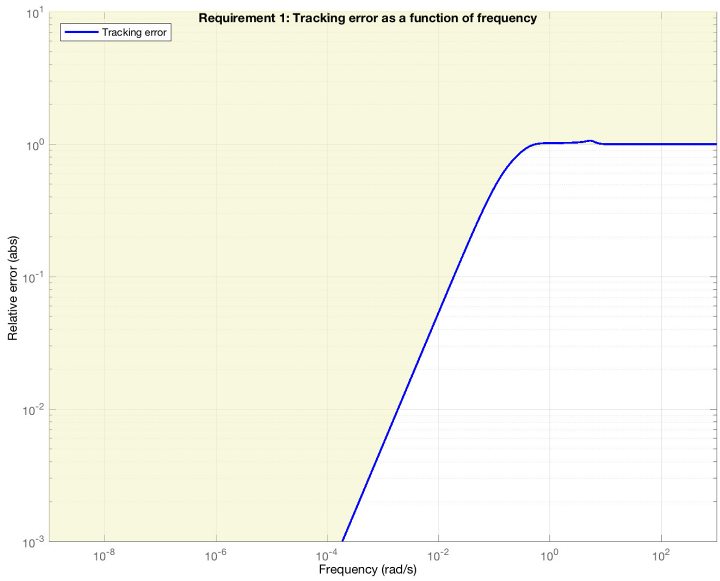

(a) Tracking requirement

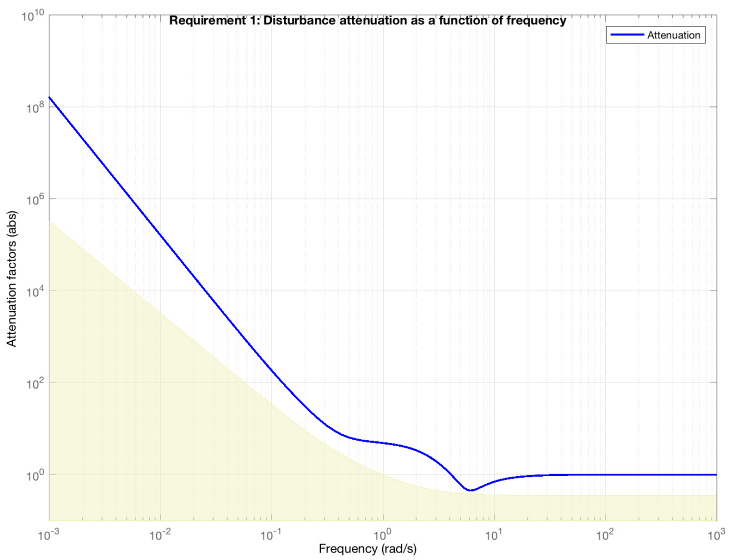

(b) Disturbance rejection requirement

Figure 7 – H_∞ requirements and achieved closed-loop performance (quadrotor platform).

DOI: 10.13009/EUCASS2017-472

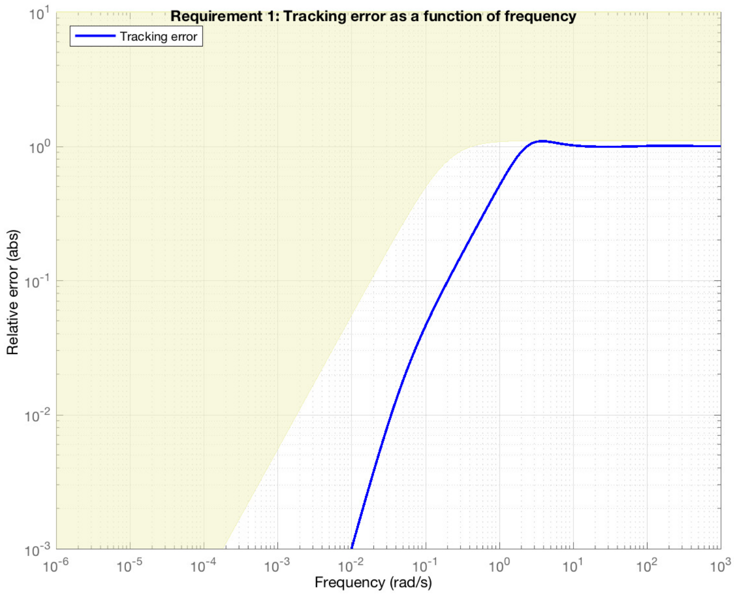

(a) Tracking requirement

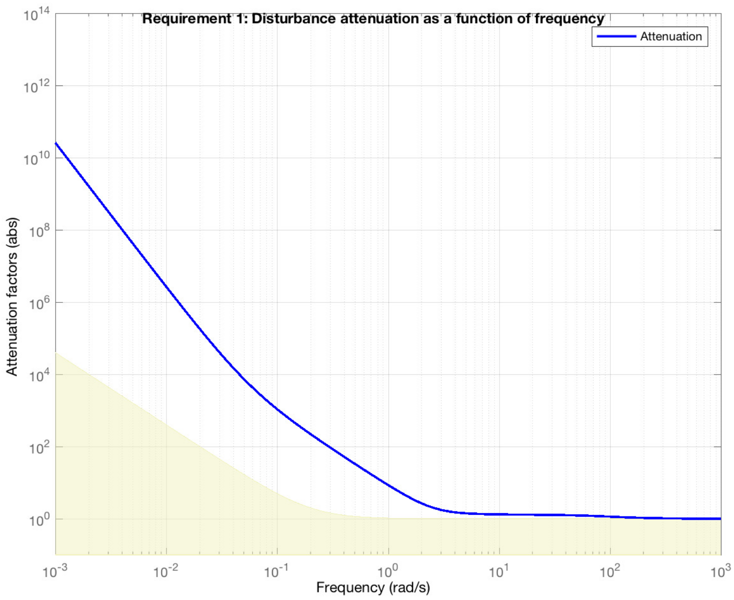

(b) Disturbance rejection requirement

Figure 8 – H_∞ requirements and achieved closed-loop performance (tilt-arm platform).

5. Simulation results

To validate the controller tuning, some simulations in the Matlab/Simulink environment have been carried out. The proposed architecture has been tested in various conditions depending on the possible noises or disturbances which may act on the multirotors. The desired trajectory provides an initial take-off and a first translation in the North direction; once the proximity sensor detects the presence of the wall, distance control is activated and surface is "locked" at a fixed distance (1 m), even if the setpoint imposed by the user is larger. In this regard, the scanning of an edged surface has been simulated, in order to verify the effective distance hold performance of the platforms. A translation in the East direction, parallel to the wall, is also set, just like it might be in a real scanning mission.

External disturbances such as turbulence and wind gusts as modeled in Section 2.4 by a predominant North wind have been simulated in order to verify that the control laws can reduce the effect of disturbances and that the risk of collision between the wall and UAV is very unlikely.

The simulation results for the quadrotor, as shown in Figure 9, demonstrate that the oscillation from the target North position of the quadrotor increases up to a maximum of about 50 cm peak error, which is still an acceptable displacement considering that the quadrotor is flying in a light turbulence wind field and has therefore a safety margin of another 50 cm from the wall, and then it settles between 20 and 30 cm when the control is activated. East position, for same reason of before, is affected of quite obvious oscillatory behavior.

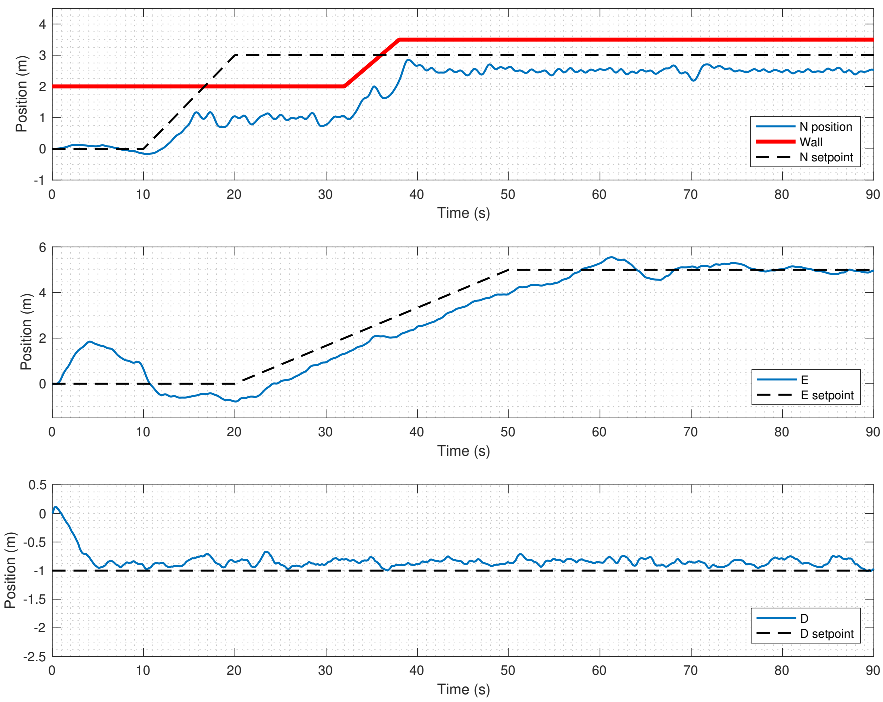

Figure 9 – Simulated trajectory in windy conditions (quadrotor platform).

The performance of the tilt-arm platform is illustrated in Figure 10, from which it can be seen that in windy conditions the tilt-arm is shifted up to a maximum of 45 cm from the target North position as soon as the control is activated, but subsequently settles on more than acceptable values with maximum peaks of about 20 cm. Larger variations, but still lower than the corresponding quadrotor quantities, are detected in East direction.

Errors in North and East position with and without wind are compared and shown in Figures 11 and 12 for the quadrotor and the tilt-arm, respectively. The figures show even more clearly that the tilt-arm platform can provide superior position tracking and disturbance rejection performance.

As for attitude, it can be seen from Figure 13 that the two platforms react quite differently in the distance control task. More precisely, while the time history of the roll angle is comparable for the two platforms, the same can not be said for the pitch and yaw angles. In fact, as was expected, the quadrotor performs the distance control task by varying in a significant way the pitch attitude. The tilt-arm platform, on the other hand, operates not by varying the attitude but simply by changing the tilt angle of the arms, and therefore has a more stable response in the horizontal plane, which makes it preferable for this kind of applications. Note that in the tilt-arm simulations a slow but still inconvenient variation of the yaw angle is visible, which can lead to a misalignment with the surface, and then to an imperfect reading from the proximity sensor. The cause of this yaw oscillation is th lack of the implemented position control law

DOI: 10.13009/EUCASS2017-472

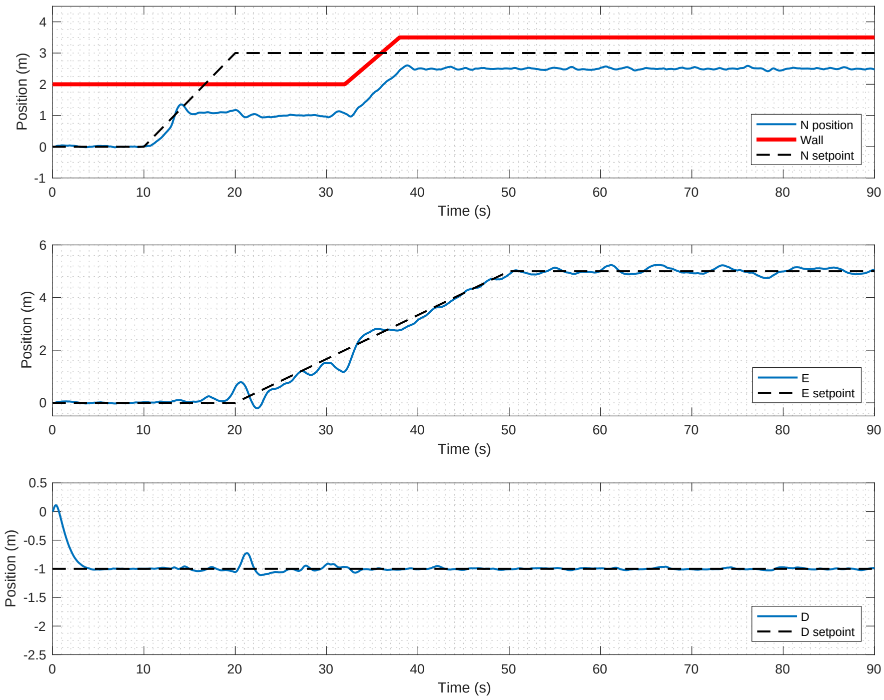

Figure 10 – Simulated trajectory in windy conditions (tilt-arm platform).

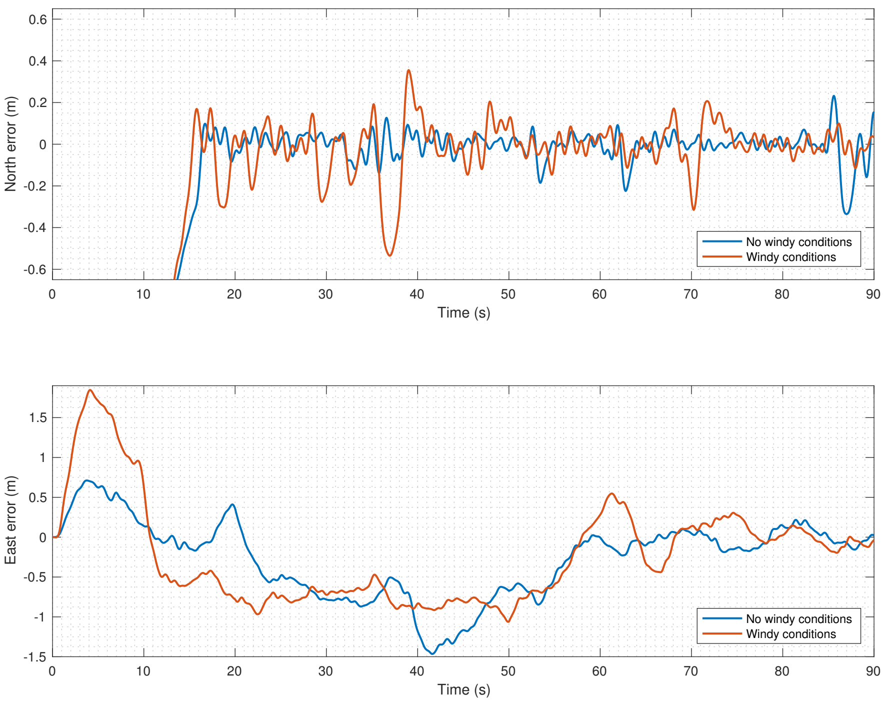

Figure 11 – Errors in N-E position (quadrotor platform).

DOI: 10.13009/EUCASS2017-472

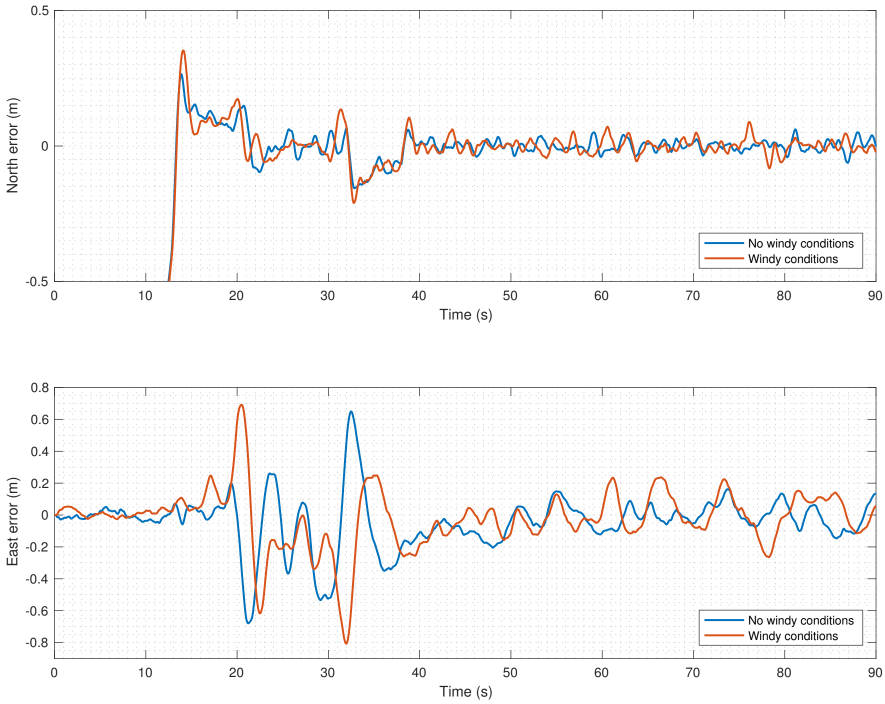

Figure 12 – Errors in N-E position (tilt-arm platform).

of a compensation term for the gyroscopic moments induced by the tilt of the platform's arms. It is expected that the yaw oscillation can be significantly reduced by means of a nonlinear compensation of this dynamic cupling effect.

Finally, the control effort is analysed. Figure 14 shows the control variable of the control system in the quadrotor case. It can be seen that in the case of nominal flight the pitch angle decreases to zero in an oscillatory exponential trend after the control is activated. In case of disturbances, the trend remains oscillatory for the whole flight thus requiring continuous attitude adjustments.

Figure 15 shows the control variable of the control system in the tilt-arm case. It is interesting to note that in general the longitudinal force in case of windy conditions is a bit lower than the same in calm air: this happens because the simulated wind is directed as the longitudinal axis of the aircraft and therefore the controller must generate a force opposite to the motion which brings it back to the desired position.

6. Concluding remarks

In this paper the problem of designing and implementing a position-hold control mode for a multirotor platform, suitable for close inspection of a large civil structure in the presence of wind has been considered. The relative merits of a conventional quadrotor platform and of a more complex tilt-arm platform have been analysed and discussed.

References

[1] E. M. A. Moutinho and F. Cunha. The tilt-quadrotor: concept, modeling and identification. *IEEE International Conference on Autonomous Robot Systems and Competitions*, 2015.

[2] A. Aboudonia, R. Rashad, and A. El-Badawy. Time domain disturbance observer based control of a quadrotor unmanned aerial vehicle. In *XXV International Conference on Information, Communication and Automation Technologies (ICAT), Sarajevo, Bosnia and Herzegovina*, 2015.

[3] P. Apkarian and D. Noll. Nonsmooth H_∞ synthesis. *IEEE Transactions on Automatic Control*, 51(1):71–86, 2006.

[4] M. Giurato. *Design, integration and control of a multirotor UAV platform*. Master's thesis, Politecnico di Milano, 2015.

[5] W. Johnson. *Helicopter Theory*. Dover Publications, New York, 1994.

DOI: 10.13009/EUCASS2017-472

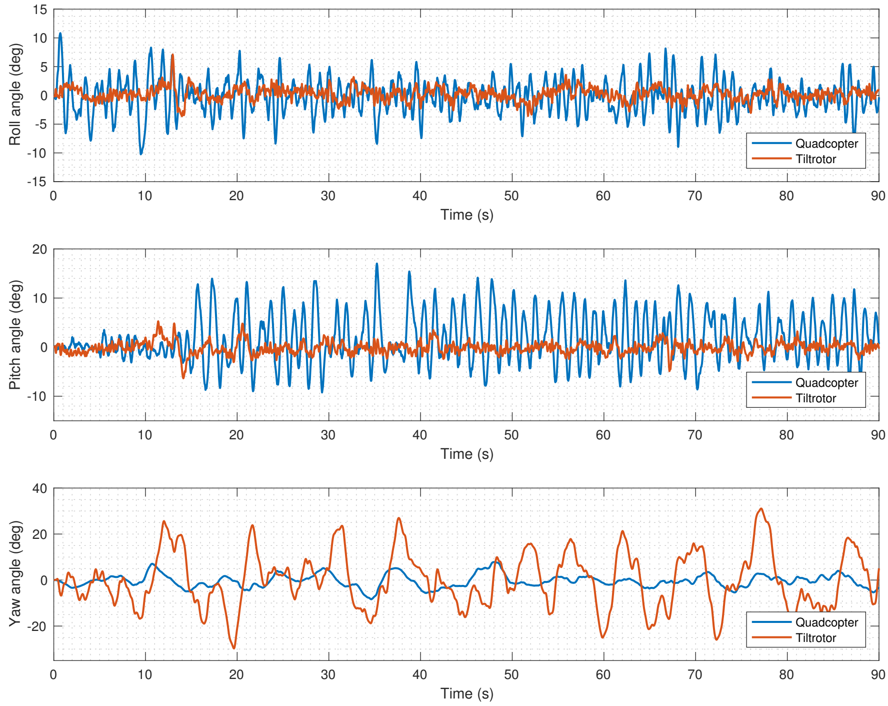

Figure 13 – Attitude angles in windy conditions.

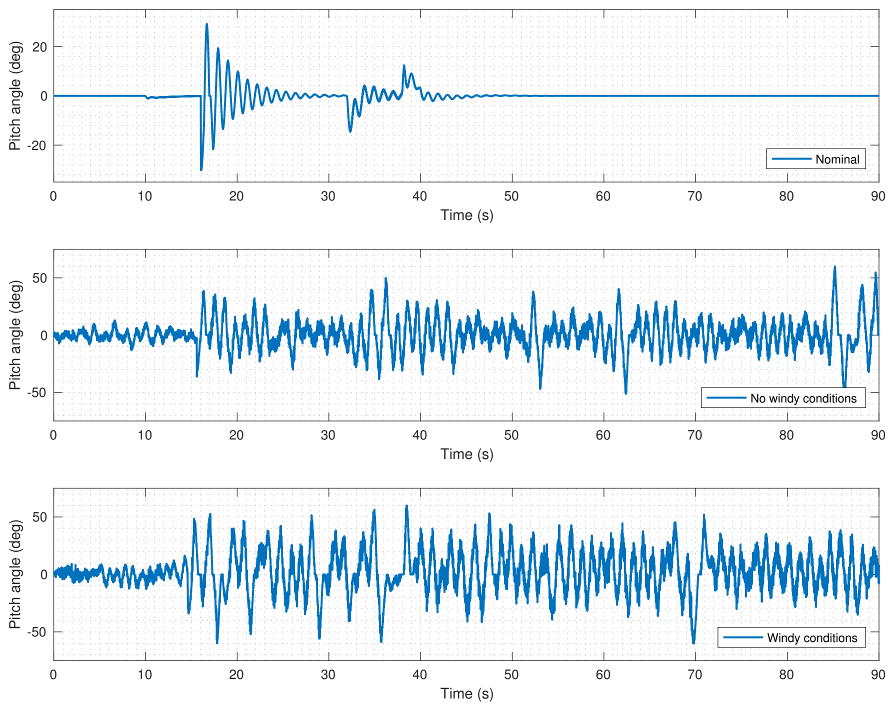

Figure 14 – Control variable (conventional quadrotor).

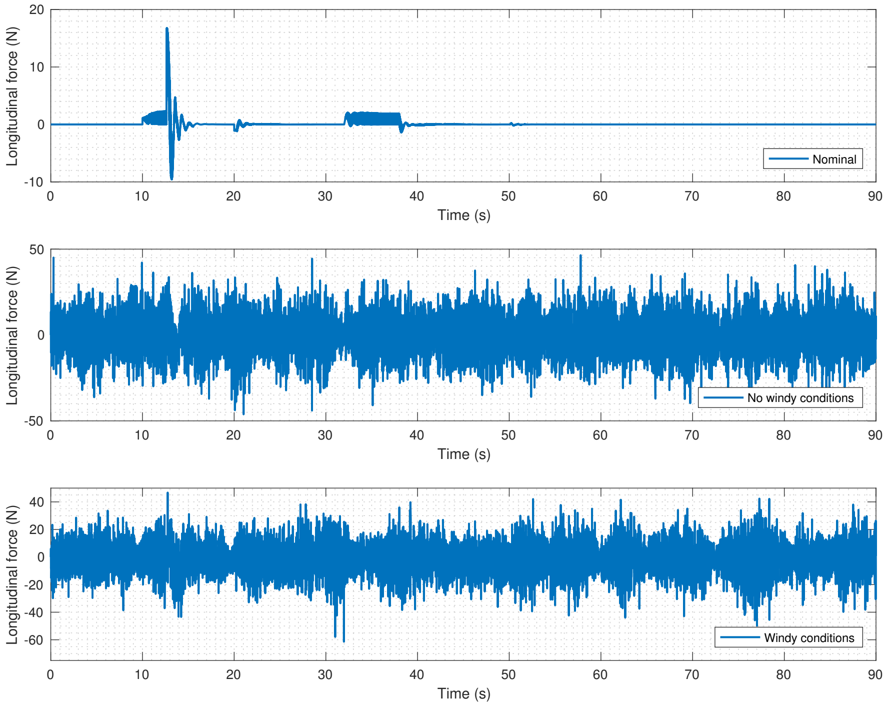

Figure 15 – Control variable (tilt-arm).

[6] V. Kumar and N. Michael. Opportunities and challenges with autonomous micro aerial vehicles. In *Springer Tracts in Advanced Robotics*, pages 41–58. Springer Nature, aug 2016.

[7] Mathworks. *Aerospace wind model*.

[8] F. A. Morrison. *Data correlation for Drag Coefficient for Sphere*. Department of Chemical Engineering, Michigan Technological University, 2013.

[9] U. D. of Defense. *MIL-F-8785C, Flying qualities of piloted airplanes*. 1980.

[10] M. Ryll, H. H. Bülthoff, and P. Robuffo Giordano. A novel overactuated quadrotor unmanned aerial vehicle: Modeling, control, and experimental validation. *IEEE Transactions on Control Systems Technology*, Volume 23:540 – 556, March 2015.

[11] K. P. Valavanis, editor. *Advances in Unmanned Aerial Vehicles - State of the Art and the Road to Autonomy*. Springer, 2007.